

# Task-oriented Uncertainty Collaborative Learning for Label-Efficient Brain Tumor Segmentation

Zhenxuan Zhang<sup>1\*</sup>, Hongjie Wu<sup>2\*</sup>, Jiahao Huang<sup>1,3</sup>, Baihong Xie<sup>6</sup>, Zhifan Gao<sup>6</sup>, Junxian Du<sup>1</sup>, Pete Lally<sup>1</sup>, and Guang Yang<sup>1,3,4,5</sup>

<sup>1</sup> Bioengineering Department and Imperial-X, Imperial College London, London W12 7SL, UK

<sup>2</sup> Department of Computing, Imperial College London, London SW7 2AZ, UK

<sup>3</sup> National Heart and Lung Institute, Imperial College London, London SW7 2AZ, UK

<sup>4</sup> Cardiovascular Research Centre, Royal Brompton Hospital, London SW3 6NP, UK

<sup>5</sup> School of Biomedical Engineering & Imaging Sciences, King's College London, London WC2R 2LS, UK

<sup>6</sup> School of Biomedical Engineering, Sun Yat-sen University, Guangzhou 510006, China

`g.yang@imperial.ac.uk`

**Abstract.** Multi-contrast magnetic resonance imaging (MRI) plays a vital role in brain tumor segmentation and diagnosis by leveraging complementary information from different contrasts. Each contrast highlights specific tumor characteristics, enabling a comprehensive understanding of tumor morphology, edema, and pathological heterogeneity. However, existing methods still face the challenges of multi-level specificity perception across different contrasts, especially with limited annotations. These challenges include data heterogeneity, granularity differences, and interference from redundant information. To address these limitations, we propose a Task-oriented Uncertainty Collaborative Learning (TUCL) framework for multi-contrast MRI segmentation. TUCL introduces a task-oriented prompt attention (TPA) module with intra-prompt and cross-prompt attention mechanisms to dynamically model feature interactions across contrasts and tasks. Additionally, a cyclic process is designed to map the prediction back to the prompt to ensure that the prompts are effectively utilized. In the decoding stage, the TUCL framework proposes a dual-path uncertainty refinement (DUR) strategy which ensures robust segmentation by refining predictions iteratively. Extensive experimental results on limited labeled data demonstrate that TUCL significantly improves segmentation accuracy (88.2% in Dice and 10.853 mm in HD95). It shows that TUCL has the potential to extract multi-contrast information and reduce the reliance on extensive annotations. The code is available at: [https://github.com/Zhenxuan-Zhang/TUCL\\_BrainSeg](https://github.com/Zhenxuan-Zhang/TUCL_BrainSeg).

**Keywords:** Segmentation · Uncertainty Estimation · Prompt Learning.

---

\* Equal contribution.

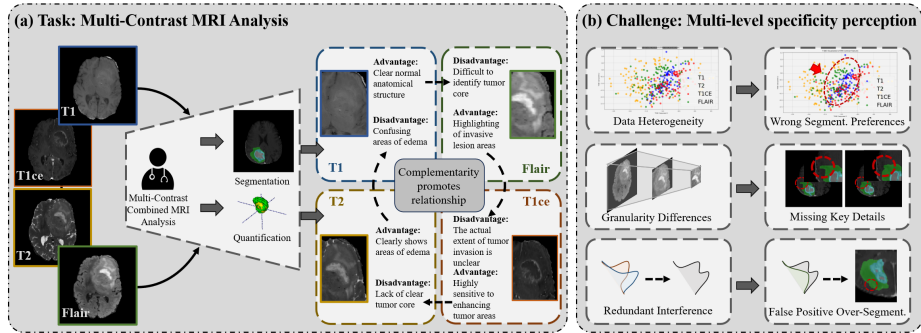


**Fig. 1.** Motivation of our TUCL framework. (a) Task: Multi-Contrast MRI Analysis. It aims to leverage complementary information from T1, T1ce, T2, and FLAIR contrasts for segmentation and further quantification. (b) Challenge: Multi-Level Specificity. It aims to address the challenge of data heterogeneity, granularity differences, and redundant interference to improve analysis accuracy.

## 1 Introduction

Multi-contrast collaborative analysis in magnetic resonance imaging (MRI) is crucial for brain tumor segmentation and diagnosis [26,18]. In clinical practice, multi-contrast modalities include T1-weighted, T2-weighted, fluid-attenuated inversion recovery (FLAIR), contrast-enhanced T1-weighted imaging (T1ce), etc [12]. These modalities allow clinicians to gain a more comprehensive understanding of tumor morphology, edema, and pathological heterogeneity (e.g., FLAIR is particularly effective in delineating peritumoral edema) [27,23]. The accurate segmentation of the tumor region can further assist in quantifying tumor volume and edema volume [10]. These aspects are critical for accurate diagnosis, surgical planning, and radiotherapy target delineation. However, manually segmenting brain tumors across multiple contrasts is labor-intensive. This limits the application of multi-contrast MRI in tumor segmentation and diagnosis [27,1,10,20]. Furthermore, obtaining high-quality annotations for all contrasts is costly and time-consuming. As a result, label-efficient segmentation approaches that can effectively utilize limited annotated data while leveraging the complementary information from multi-contrast MRI are highly desirable [14]. There is a need to design automated methods that leverage the information provided by multi-contrast MRI for robust and precise tumor segmentation while reducing annotation burdens.

However, collaborative analysis of multi-contrast MRI data still faces significant challenges related to multi-level specificity perception [21,25,9,27]. These challenges primarily stem from three aspects: data heterogeneity, granularity differences, and redundant information interference. Firstly, data heterogeneity arises due to the inherent differences between various MRI contrasts. These modalities capture unique aspects of tumor features (e.g., T1 weighted contrast provides clear anatomical structures) [27,1]. These contrasts exhibit different

sensitivities to specific tissue types, making it challenging to integrate different data sources into a unified representation without losing clinical information. Secondly, granularity differences come from different reflections on tumor details. It may affect the fusion of fine-textured microstructures to broader-scale anatomical features (e.g., the fine structural details of a tumor core may be more clearly visible in T1ce images). It requires the appropriate perception of these differences without distorting key tumor information. Third, redundant information interference presents a significant barrier in multi-contrast MRI analysis (e.g., T1- and T2-weighted images might highlight similar tumor boundaries). It leads to potential redundancies in the data. These redundancies may lead to unnecessary or conflicting features that may affect the accuracy of tumor segmentation.

Existing methods struggle to effectively address these challenges. Traditional methods (e.g., simple concatenation or early fusion) fail to capture the complex interactions among different contrasts [22]. These methods treat each contrast as an independent source of information, which overlooks the contextual relationships between them [19]. This results in an incomplete representation of the tumor. Recent methods like multi-contrast cross attention mechanisms still have limitations in balancing the contributions of each image contrast [11,8]. These methods often focus on global feature alignment but may miss the importance of task-specific refinements (e.g. specific tumor region details might be more clearly visible in one contrast but harder to detect in others) [24]. In these cases, they fail to preserve the nuanced and localized details that are essential for accurate segmentation [4]. This can lead to inaccurate tumor boundaries or incorrect identification of regions of necrosis. Lastly, existing methods may not handle the redundancy interaction of multi-contrast data due to the lack of constraints on redundant boundaries [15,3]. The redundant features can be amplified and cause conflicting features (i.e. similar tumor boundaries in two contrasts are interpreted differently and cause inconsistent segmentation).

In this paper, we propose a Task-oriented Uncertainty Collaborative Learning (TUCL) framework (Fig. 2). Compared with previous multi-input concatenation or contrast-cross attention mechanisms, we propose a task-oriented prompt and uncertainty collaborative learning mechanism. This dynamically models the contextual relationship between multi-contrast input and multi-task output (MIMO) through the task-oriented prompt module, rather than relying solely on feature aggregation. The cycle mapping from output prediction to text-prompt further ensures the validity of the prompt with the reverse consistency of the prediction. This makes it more robust to the case of missing modalities. Specifically, the core of our TUCL is the task-oriented prompt attention process (TPA), which consists of intra-prompt attention and cross-prompt attention. Intra-prompt attention models the multi-granularity relationships within multi-contrast and multi-region prompts independently. Cross-prompt attention fosters interaction between visual features and text prompt representations. It facilitates the collaborative learning paradigm of multi-contrast and multi-task objectives. Further, we introduce a dual-path uncertainty refinement (DUR)

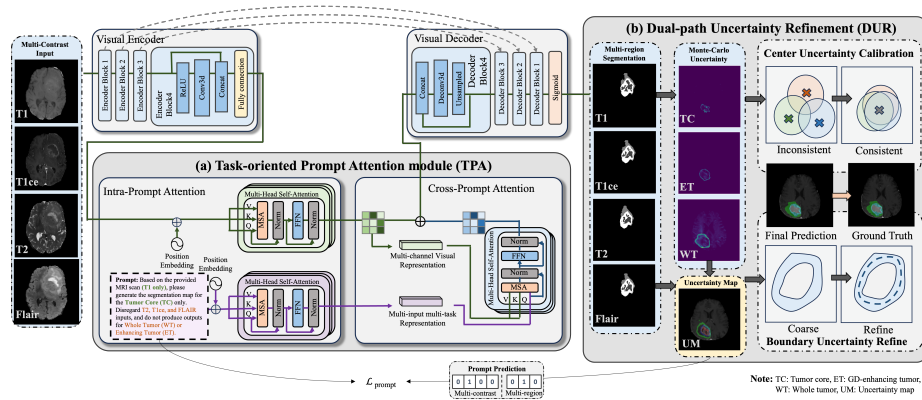


**Fig. 2.** Workflow of the proposed Task-oriented Uncertainty Collaborative Learning (TUCL) framework. (a) The Task Prompt Attention (TPA) module integrates intra-prompt and cross-prompt attention mechanisms to capture multi-region and multi-contrast features. (b) The model leverages dual-path uncertainty refinement (DUR) to enhance segmentation accuracy. It produces consistent and refined predictions compared to ground truth.

strategy to mitigate inconsistencies (i.e., center and boundary) and ambiguities in segmentation. It iteratively calibrates the region center and refines the boundary prediction to alleviate redundant information interference. The contribution of our work lies in three aspects:

- We propose a task-oriented attention prompt and uncertainty collaborative learning mechanism to address the challenge of multi-level specificity perception in multi-contrast MRI segmentation.
- We design a segmentation framework achieve efficient collaboration between multi-contrast and multi-task outputs, ensuring robust performance even in the presence of missing modalities.
- We verify the superiority of our TUCL. It significantly improves segmentation accuracy (88.2% in Dice and 10.853 mm in HD95) and outperforms SOTA methods.

## 2 Methods

**Problem Formulation** Let the multi-contrast MRI images be represented as a set of inputs  $\mathbf{X} = \{x_i\}_{i=1}^N$ , where each  $x_i \in \mathbb{R}^{4 \times W \times H \times D}$  corresponds to a multi-contrast scan. The outputs are multi-region segmentation masks  $\mathbf{Y} = \{y_j\}_{j=1}^M$ , where each  $y_j \in \mathbb{R}^{3 \times W \times H \times D}$  represents the segmented regions. Our objective is to learn a voxel-wise mapping function  $f_\theta : \mathbf{X} \rightarrow \mathbf{Y}$ , parameterized by a deep neural network. The function is defined within a hypothesis space  $\mathcal{H}$ , formulated as:

$$\mathcal{H} = \{f_\theta \mid f : \mathbf{X} \rightarrow \mathbf{Y}, \theta \in \Theta\} \quad (1)$$

**Table 1.** Quantitative comparison on BraTS 2021 dataset with different labeled ratios.

Ratio	Method	Param FLOPs		Dice (%) $\uparrow$				HD95 (mm) $\downarrow$			
		(M)	(G)	ET	WT	TC	Ave	ET	WT	TC	Ave
10%	UNet [16]	1.98	16.49	66.4	86.6	81.7	78.2	18.306	15.877	17.002	17.395
	Att-UNet [2]	5.91	407.48	75.9	84.1	83.2	81.1	18.148	12.626	19.750	16.175
	SegResNet[7]	4.70	596.73	70.1	84.3	82.5	78.9	20.462	15.898	19.676	18.012
	Vnet[13]	45.61	3014.13	66.9	80.4	74.7	74.0	19.864	22.050	19.423	20.112
	TransBTS [20]	32.99	1305.92	74.1	78.7	82.2	78.3	11.739	16.796	11.977	13.171
	UNETR [6]	131.97	796.87	75.4	81.4	75.1	77.3	17.106	13.225	20.602	16.311
	Swin-UNETR [5]	62.19	3073.72	73.5	85.5	79.5	79.5	19.830	18.152	21.203	19.728
	MedNext[17]	6.59	1009.47	79.0	87.1	87.6	84.6	17.846	14.471	18.392	16.903
	Ours (w/o T1)	-	-	77.8	88.5	88.8	85.0	15.922	16.087	15.175	15.728
	Ours (w/o T2)	-	-	77.7	83.2	85.1	82.0	15.884	24.039	16.482	18.802
	Ours (w/o T1ce)	-	-	67.5	88.2	55.8	70.5	18.682	<b>8.425</b>	16.552	14.553
	Ours (w/o Flair)	-	-	75.8	78.7	84.0	79.5	27.654	40.144	29.364	32.387
	Ours	33.38	326.8	<b>80.5</b>	<b>89.1</b>	<b>88.9</b>	<b>86.2</b>	<b>13.398</b>	14.524	<b>12.715</b>	<b>13.546</b>
30%	UNet [16]	1.98	16.49	76.4	89.3	81.3	82.3	18.612	15.209	21.127	18.316
	Att-UNet [2]	5.91	407.48	77.9	86.5	84.1	82.8	17.733	15.880	20.016	17.876
	SegResNet[7]	4.70	596.73	78.0	83.6	80.9	80.8	17.061	14.679	18.355	16.698
	Vnet[13]	45.61	3014.13	76.4	77.2	82.9	78.8	12.901	27.421	14.133	18.818
	TransBTS [20]	32.99	1305.92	76.6	88.3	87.5	84.1	18.328	20.555	17.188	18.357
	UNETR [6]	131.97	796.87	73.8	86.5	80.9	80.4	20.700	17.523	22.598	20.607
	Swin-UNETR [5]	62.19	3073.72	75.2	87.7	76.7	79.8	23.475	17.154	27.443	22.357
	MedNext[17]	6.59	1009.47	<b>82.6</b>	<b>91.4</b>	90.6	88.2	10.914	<b>10.523</b>	10.348	10.595
	Ours (w/o T1)	-	-	79.7	73.3	89.2	80.7	12.639	20.793	13.474	15.635
	Ours (w/o T2)	-	-	82.3	88.5	87.0	85.9	<b>10.342</b>	18.294	11.370	13.335
	Ours (w/o T1ce)	-	-	54.5	89.6	47.4	63.8	17.303	15.111	17.412	16.609
	Ours (w/o Flair)	-	-	75.2	77.4	84.1	78.9	19.835	19.628	19.179	19.547
	Ours	33.38	326.8	81.0	91.3	<b>92.3</b>	<b>88.2</b>	10.779	12.202	<b>9.577</b>	<b>10.853</b>

where  $\Theta$  represents the parameter space. The optimal parameters  $\theta^*$  are obtained by minimizing a voxel-wise loss function  $\mathcal{L}$ , leading to the following optimization problem:

$$\theta^* = \arg \min_{\theta \in \Theta} \mathbb{E}_{\mathbf{X} \sim \mathcal{P}_X, \mathbf{Y} \sim \mathcal{P}_Y} [\mathcal{L}(f_\theta(\mathbf{X}), \mathbf{Y})] \quad (2)$$

where  $\mathcal{P}_X$  and  $\mathcal{P}_Y$  denote the underlying distributions of the multi-contrast inputs and the corresponding segmentation outputs, respectively.

**Task-oriented Prompt Attention Module (TPA)** Our framework centers on a Task-oriented Prompt Attention (TPA) module that guides multi-contrast, multi-region segmentation in a task-specific manner (Fig. 2(a)). The TPA module consists of two components. First, intra-prompt Attention refines both the segmentation features  $f_{\text{seg}}$  and the prompt features  $X_{\text{prompt}}$ , producing specialized representations for different contrasts and regions. Second, cross-prompt Attention fuses the refined features from both streams, enabling the prompt to steer the segmentation process and enforce consistency across modalities. This can be formally defined as:

$$f_{\text{TPA}} = \text{CrossAttn}\left(\text{IntraAttn}(f_{\text{seg}}), \text{IntraAttn}(X_{\text{prompt}})\right). \quad (3)$$

**Table 2.** Ablation study for different modules (TPA, DUR).

Ratio	Modules			Dice (%) $\uparrow$				HD95 (mm) $\downarrow$			
	Base.	TPA	DUR	ET	WT	TC	Ave	ET	WT	TC	Ave
10%	$\checkmark$	-	-	63.9	88.3	83.4	78.5	26.190	14.725	16.429	19.115
	$\checkmark$	$\checkmark$	-	77.1	85.2	82.2	81.5	17.806	16.534	17.775	17.37
	$\checkmark$	$\checkmark$	$\checkmark$	<b>80.5</b>	<b>89.1</b>	<b>88.9</b>	<b>86.1</b>	<b>13.398</b>	<b>14.524</b>	<b>12.715</b>	<b>13.55</b>
30%	$\checkmark$	-	-	78.7	88.4	83.7	83.6	20.126	12.488	21.963	18.19
	$\checkmark$	$\checkmark$	-	<b>81.7</b>	84.6	86.1	84.1	11.748	27.017	11.900	16.89
	$\checkmark$	$\checkmark$	$\checkmark$	81.0	<b>91.3</b>	<b>92.3</b>	<b>88.2</b>	<b>10.779</b>	<b>12.202</b>	<b>9.577</b>	<b>10.85</b>

To further validate the effectiveness of the TPA module, we introduce a Task-Oriented Cycle mechanism. In this mechanism, refined segmentation predictions are fed back to update the prompt features, forming a cyclic process that iteratively enhances performance. This cycle is enforced by the following loss function:

$$\mathcal{L}_{\text{TPA}} = \mathbb{E}_{x \in X, \hat{y} \in \hat{Y}} \left[ \left\| X_{\text{prompt}} - \Phi(F(X_{\text{prompt}}), \hat{y}) \right\|^2 \right], \quad (4)$$

where  $\Phi(\cdot, \cdot)$  is an update function that remaps the extracted prompt features  $F(X_{\text{prompt}})$  with the prediction  $\hat{y}$  back to the prompt space. This cyclic feedback reinforces robust prompt learning and serves as a consistency constraint, validating the TPA module’s guidance in segmentation.

**Dual-path Uncertainty Refinement** We employ dual uncertainty refinement to further refine the segmentation center and boundary. The uncertainty map uses Monte Carlo sampling to estimate pixel-by-pixel uncertainty during inference. Specifically, multiple stochastic forward passes yield a set of predictions  $\{\hat{Y}^{(t)}\}_{t=1}^T$ , from which the uncertainty map  $U$  is computed as:

$$U = \frac{1}{T} \sum_{t=1}^T (\hat{Y}^{(t)} - \frac{1}{T} \sum_{k=1}^T \hat{Y}^{(k)})^2, \quad (5)$$

where  $T$  is the number of sampling runs. The resulting uncertainty map highlights regions with inconsistent predictions. We estimate pixel-wise uncertainty via Monte Carlo sampling and partition the image domain  $\Omega$  into core and boundary regions:  $\Omega_c = \{p \in \Omega \mid U(p) \leq \delta\}$ ,  $\Omega_b = \{q \in \Omega \mid U(q) > \delta\}$ , where  $U(p)$  is the uncertainty at voxel  $p$  and  $\delta$  is a pre-defined threshold. The final loss function integrates two levels of uncertainty optimization into a unified loss.

$$\mathcal{L}_{\text{DUR}} = \alpha \cdot \frac{1}{|\Omega_c|} \sum_{p \in \Omega_c} \ell(\hat{Y}(p), Y(p)) + \beta \cdot \frac{1}{|\Omega_b|} \sum_{q \in \Omega_b} \ell(\hat{Y}(q), Y(q)), \quad (6)$$

where  $\ell(\cdot, \cdot)$  is the overlap loss, and  $\alpha, \beta$  are weighting factors balancing the center and boundary constraints.

**Overall Loss Function** : The overall loss function integrates all the components described above to achieve joint optimization of segmentation accuracy and uncertainty refinement. The total loss  $\mathcal{L}_{\text{total}}$  is formulated as:

$$\mathcal{L}_{\text{total}} = \lambda_1 \mathcal{L}_{\text{seg}} + \lambda_2 \mathcal{L}_{\text{TPA}} + \lambda_3 \mathcal{L}_{\text{DUR}}, \quad (7)$$

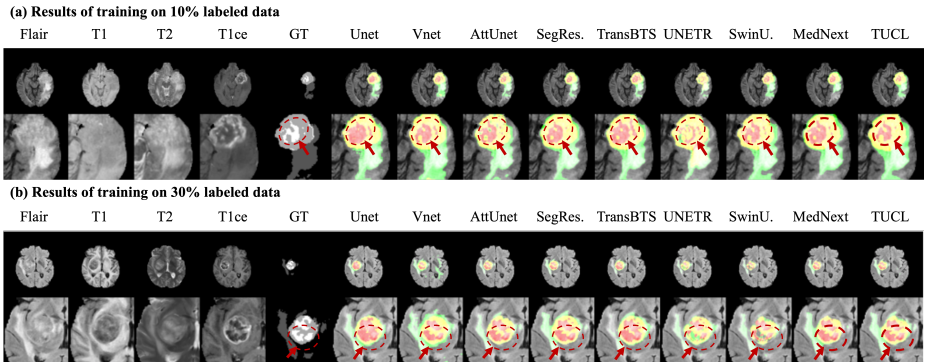


**Fig. 3.** Comparison of brain tumor segmentation results with (a) 10% and (b) 30% labeled data. The first five columns show multi-contrast MRI inputs and ground truth, while the rest display segmentation results from different methods.

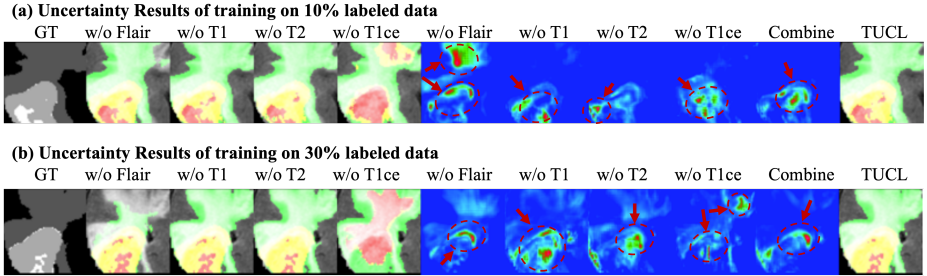


**Fig. 4.** Uncertainty visualization of multi-contrast MRI segmentation. (a) and (b) show the results with 10% and 30% labeled data, respectively. The uncertainty maps highlight regions with higher prediction variability across different contrast removals.

where  $\lambda_1, \lambda_2, \lambda_3$  are hyperparameters determined empirically to control the contributions of each loss term.

### 3 Experiment

**Dataset:** We use the public BRATS2021 dataset [1] to evaluate the performance. The BRATS2021 dataset contains MRI data from 2040 subjects with brain tumors. The segmentation annotations comprise the GD-enhancing tumor (ET — label 4), the peritumoral edematous/invaded tissue (ED — label 2), and the necrotic tumor core (NCR — label 1). The whole tumor (WT) as the union of ED, NCR, and ET; the tumor core (TC) as the union of NCR and ET.

**Metric:** We evaluate the segmentation performance of our TUCL framework using several key metrics. These include: 1) Dice Similarity Coefficient (Dice), which measures the spatial overlap between predicted and ground truth regions. 2) 95th Percentile Hausdorff Distance (HD95) to assess boundary agreement by

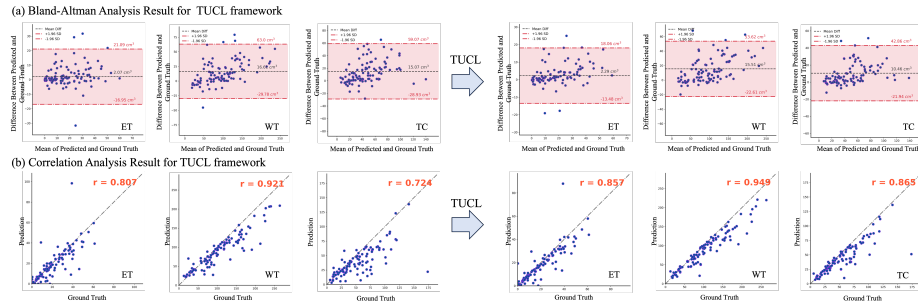


**Fig. 5.** Bland-Altman and correlation plots of predicted versus ground truth tumor volumes. (a) The x-axis shows the mean of the predicted and true volumes, while the y-axis shows their difference; dashed lines indicate the mean bias and 95% limits of agreement. (b) The x-axis represents the true volumes, and the y-axis represents the predicted volumes.

quantifying the maximum distance between segmentation boundaries.

**Comparison Experiment:** Table 1 and Fig. 3 demonstrate the superior performance of our TUCL framework in brain tumor segmentation. TUCL achieves a Dice score of 86.2% and an HD95 of 13.546 mm with 10% labeled data, improving to 88.2% and 10.853 mm with 30% labeled data. Removing MRI modalities degrades performance, with Dice dropping to 85.0% (without T1), 82.0% (without T2), and 70.5% (without T1ce). These results indicate that TUCL consistently provides more accurate tumor delineation than most SOTA models, preserving fine structures and achieving competitive Dice and HD95 scores.

**Ablation Study:** Fig. 4 highlights increased prediction variability when specific modalities are excluded. Higher uncertainty regions, particularly in tumor boundaries, indicate the importance of T1ce and FLAIR for precise delineation. The reduction in uncertainty with 30% labeled data suggests improved model confidence with more supervision. These findings align with Table 2, where incorporating the TPA and DUR modules enhances segmentation accuracy.

**Clinical Metric Evaluation:** Fig. 5 demonstrates the TUCL framework’s strong predictive consistency across different tumor sub-regions. The Bland-Altman analysis (Fig. 5a) further confirms reduced bias and narrower limits of agreement, highlighting TUCL’s substantial performance enhancement in tumor volume estimation. The correlation analysis (Fig. 5b) shows high agreement, with  $r$ -values improving from 0.724 to 0.865 (TC) and from 0.807 to 0.857 (ET) after integrating TUCL.

## 4 Conclusion

In this paper, we propose the Task-oriented Uncertainty Collaborative Learning (TUCL) framework to address multi-level specificity challenges in multi-contrast

MRI brain tumor segmentation. TUCL integrates task-aware prompt attention and dual-path uncertainty calibration, achieving state-of-the-art performance (Dice: 88.2%, HD95: 10.853 mm). Although our TUCL achieves strong performance in MRI brain tumor segmentation, it still has some limitations. The TUCL needs to be extended to other diseases (e.g., Parkinson’s and Alzheimer’s) for broader clinical validation (e.g., CT and PET). Our future work will focus on adapting TUCL to different diseases and other imaging modalities.

## References

1. Baid, U., Ghodasara, S., Mohan, S., Bilello, M., Calabrese, E., Colak, E., Farahani, K., Kalpathy-Cramer, J., Kitamura, F.C., Pati, S., et al.: The rsna-asnr-miccai brats 2021 benchmark on brain tumor segmentation and radiogenomic classification. arXiv preprint arXiv:2107.02314 (2021)
2. Çiçek, Ö., Abdulkadir, A., Lienkamp, S.S., Brox, T., Ronneberger, O.: 3d u-net: learning dense volumetric segmentation from sparse annotation. In: Medical Image Computing and Computer-Assisted Intervention—MICCAI 2016: 19th International Conference, Athens, Greece, October 17-21, 2016, Proceedings, Part II 19. pp. 424–432 (2016)
3. De Sutter, S., Wuts, J., Geens, W., Vanbinst, A.M., Duerinck, J., Vandemeulebroucke, J.: Modality redundancy for mri-based glioblastoma segmentation. International journal of computer assisted radiology and surgery pp. 2101–2109 (2024)
4. Dolz, J., Gopinath, K., Yuan, J., Lombaert, H., Desrosiers, C., Ayed, I.B.: Hyperdense-net: a hyper-densely connected cnn for multi-modal image segmentation. IEEE transactions on medical imaging pp. 1116–1126 (2018)
5. Hatamizadeh, A., Nath, V., Tang, Y., Yang, D., Roth, H.R., Xu, D.: Swin unetr: Swin transformers for semantic segmentation of brain tumors in mri images. In: International MICCAI brainlesion workshop. pp. 272–284 (2021)
6. Hatamizadeh, A., Tang, Y., Nath, V., Yang, D., Myronenko, A., Landman, B., Roth, H.R., Xu, D.: Unetr: Transformers for 3d medical image segmentation. In: Proceedings of the IEEE/CVF winter conference on applications of computer vision. pp. 574–584 (2022)
7. Hsu, C., Chang, C., Chen, T.W., Tsai, H., Ma, S., Wang, W.: Brain tumor segmentation (brats) challenge short paper: Improving three-dimensional brain tumor segmentation using segresnet and hybrid boundary-dice loss. In: International MICCAI Brainlesion Workshop. pp. 334–344 (2021)
8. Huang, S., Li, J., Mei, L., Zhang, T., Chen, Z., Dong, Y., Dong, L., Liu, S., Lyu, M.: Accurate multi-contrast mri super-resolution via a dual cross-attention transformer network. In: International Conference on Medical Image Computing and Computer-Assisted Intervention. pp. 313–322 (2023)
9. Huang, Y., Du, C., Xue, Z., Chen, X., Zhao, H., Huang, L.: What makes multi-modal learning better than single (provably). Advances in Neural Information Processing Systems pp. 10944–10956 (2021)
10. Jiang, Y., Zhang, Y., Lin, X., Dong, J., Cheng, T., Liang, J.: Swinbts: A method for 3d multimodal brain tumor segmentation using swin transformer. Brain sciences p. 797 (2022)
11. Li, G., Zhao, L., Sun, J., Lan, Z., Zhang, Z., Chen, J., Lin, Z., Lin, H., Xing, W.: Rethinking multi-contrast mri super-resolution: Rectangle-window cross-attention

- transformer and arbitrary-scale upsampling. In: 2023 IEEE/CVF International Conference on Computer Vision (ICCV). pp. 21173–21183 (2023)
12. Lin, H., Xiao, H., Dong, L., Teo, K.B.K., Zou, W., Cai, J., Li, T.: Deep learning for automatic target volume segmentation in radiation therapy: a review. *Quantitative Imaging in Medicine and Surgery* p. 4847 (2021)
  13. Milletari, F., Navab, N., Ahmadi, S.A.: V-net: Fully convolutional neural networks for volumetric medical image segmentation. In: 2016 fourth international conference on 3D vision (3DV). pp. 565–571 (2016)
  14. Nie, D., Wang, L., Xiang, L., Zhou, S., Adeli, E., Shen, D.: Difficulty-aware attention network with confidence learning for medical image segmentation. In: Proceedings of the AAAI Conference on Artificial Intelligence. pp. 1085–1092 (2019)
  15. Rahman Siddiquee, M.M., Myronenko, A.: Redundancy reduction in semantic segmentation of 3d brain tumor mris. In: International MICCAI Brainlesion Workshop. pp. 163–172 (2021)
  16. Ronneberger, O., Fischer, P., Brox, T.: U-net: Convolutional networks for biomedical image segmentation. In: Medical image computing and computer-assisted intervention—MICCAI 2015: 18th international conference, Munich, Germany, October 5–9, 2015, proceedings, part III 18. pp. 234–241 (2015)
  17. Roy, S., Koehler, G., Ulrich, C., Baumgartner, M., Petersen, J., Isensee, F., Jaeger, P.F., Maier-Hein, K.H.: Mednext: transformer-driven scaling of convnets for medical image segmentation. In: International Conference on Medical Image Computing and Computer-Assisted Intervention. pp. 405–415 (2023)
  18. Vollmuth, P., Foltyn, M., Huang, R.Y., Galldiks, N., Petersen, J., Isensee, F., van den Bent, M.J., Barkhof, F., Park, J.E., Park, Y.W., et al.: Artificial intelligence (ai)-based decision support improves reproducibility of tumor response assessment in neuro-oncology: An international multi-reader study. *Neuro-oncology* pp. 533–543 (2023)
  19. Wang, X., Li, Z., Huang, Y., Jiao, Y.: Multimodal medical image segmentation using multi-scale context-aware network. *Neurocomputing* pp. 135–146 (2022)
  20. Wenxuan, W., Chen, C., Meng, D., Hong, Y., Sen, Z., Jiangyun, L.: Transbts: Multimodal brain tumor segmentation using transformer. In: International Conference on Medical Image Computing and Computer-Assisted Intervention. pp. 109–119 (2021)
  21. Yang, H., Zhou, T., Zhou, Y., Zhang, Y., Fu, H.: Flexible fusion network for multimodal brain tumor segmentation. *IEEE Journal of Biomedical and Health Informatics* pp. 3349–3359 (2023)
  22. Zhang, G., Zhou, J., He, G., Zhu, H.: Deep fusion of multi-modal features for brain tumor image segmentation. *Heliyon* p. e19266 (2023)
  23. Zhang, Y., He, N., Yang, J., Li, Y., Wei, D., Huang, Y., Zhang, Y., He, Z., Zheng, Y.: mmformer: Multimodal medical transformer for incomplete multimodal learning of brain tumor segmentation. In: International Conference on Medical Image Computing and Computer-Assisted Intervention. pp. 107–117 (2022)
  24. Zhang, Y., He, N., Yang, J., Li, Y., Wei, D., Huang, Y., Zhang, Y., He, Z., Zheng, Y.: mmformer: Multimodal medical transformer for incomplete multimodal learning of brain tumor segmentation. In: International Conference on Medical Image Computing and Computer-Assisted Intervention. pp. 107–117 (2022)
  25. Zhang, Y., Yang, J., Tian, J., Shi, Z., Zhong, C., Zhang, Y., He, Z.: Modality-aware mutual learning for multi-modal medical image segmentation. In: Medical Image Computing and Computer Assisted Intervention—MICCAI 2021: 24th International Conference, Strasbourg, France, September 27–October 1, 2021, Proceedings, Part I 24. pp. 589–599 (2021)

26. Zhou, J., Zaiss, M., Knutsson, L., Sun, P.Z., Ahn, S.S., Aime, S., Bachert, P., Blakeley, J.O., Cai, K., Chappell, M.A., et al.: Review and consensus recommendations on clinical apt-weighted imaging approaches at 3t: application to brain tumors. *Magnetic resonance in medicine* pp. 546–574 (2022)
27. Zhu, Z., He, X., Qi, G., Li, Y., Cong, B., Liu, Y.: Brain tumor segmentation based on the fusion of deep semantics and edge information in multimodal mri. *Information Fusion* pp. 376–387 (2023)